Research Article | Vol. 28, No. 3 / 3 February 2020 / Optics Express 3636
Optics EXPRESS

Performance comparison of Yb:YAG ceramics and crystal gain material in a large-area, high-energy, high average–power diode-pumped laser

M. Divoky,[1,*] J. Pilar,[1] M. Hanus,[1] P. Navratil,[1] M. Sawicka-Chyla,[1] M. De Vido,[2] P. J. Phillips,[2] K. Ertel,[2] T. Butcher,[2] M. Fibrich,[3] J. T. Green,[3] M. Koselja,[3] J. Preclikova,[4] J. Kubat,[4] J. Houzvicka,[4] B. Rus,[3] J. Collier,[2] A. Lucianetti,[1] and T. Mocek[1]

[1]*HiLASE Centre, Institute of Physics of the Czech Academy of Sciences, Za Radnici 828, 25241 Dolní Břežany, Czech Republic*
[2]*Central Laser Facility, STFC Rutherford Appleton Laboratory, Didcot, OX11 0QX, UK*
[3]*Extreme Light Infrastructure-Beamlines, Institute of Physics of the Czech Academy of Sciences, Za Radnici 835, 25241 Dolní Břežany, Czech Republic*
[4]*CRYTUR, spol. s r.o., Na Lukách 2283, CZ-511 01 Turnov, Czech Republic*
[*]*divoky@fzu.cz*

Abstract: We compare for the first time the influence of different Yb:YAG gain media on the performance of a large-area, high average–power laser system with an output energy of up to 6 J. Monocrystalline slabs grown by a new technique without central growth defect are compared with ceramics. Small signal gain, maximum output energy and thermal lensing are compared for ceramic slabs with co-sintered amplified spontaneous emission (ASE) absorber cladding, monocrystalline slab with and without optically bonded ASE absorber cladding, and surface structured monocrystalline slabs. We show that these large monocrystals with optically bonded absorber cladding have similar performance to cladded ceramics, so far the only material for high-energy Yb:YAG lasers.

1. Introduction

High-energy, high average–power (HE-HAP) diode pumped laser systems offer unprecedented energy stability and faster processing speeds in comparison to the more established flash lamp pumped systems. The parameters of such lasers open up new application areas such as advanced material processing and laser shock peening [1,2], large area laser induced damage threshold testing, and pumping of high repetition rate ultra-high intensity femtosecond petawatt laser systems [3].

Several geometries of such HE-HAP systems have been previously considered, but as of today, only the multi-slab laser architecture has delivered pulse energies above 50 J at a 10 Hz repetition rate. The principle of a multi-slab laser system is to divide the gain medium into multiple slabs which are stacked longitudinally with gaps between within the laser head. A coolant flows between the slabs, allowing efficient heat extraction from the gain media and higher accessible average powers. The Mercury project demonstrated 61 J at 10 Hz using Yb:S-FAP crystal gain media at room temperature [4]. The HAPLS project demonstrated 97 J at 3.3 Hz using Nd:APG-1 glass as gain medium [5]. It should be noted that HAPLS will achieve a much higher energy at a 10 Hz repetition rate in the future, but it has not been demonstrated yet. The Bivoj/DiPOLE system demonstrated 105 J at 10 Hz using cryogenically cooled Yb:YAG ceramics as the gain

#379713 https://doi.org/10.1364/OE.379713
Journal © 2020 Received 15 Oct 2019; revised 10 Jan 2020; accepted 15 Jan 2020; published 27 Jan 2020

Optics EXPRESS

medium [6]. There are many more diode pumped laser systems around 10 J and 10 Hz level [7,8]. All above mentioned energies were obtained for nanosecond pulses.

The large aperture of the gain media used in such lasers limits the material choice to glass or ceramics. Also, high energy diode pumped systems suffer from amplified spontaneous emission (ASE) that decreases the gain of the system. To counter this, Sm or Cr doped ASE absorbing cladding is applied to the gain medium to prevent reflections of spontaneously emitted photons from the edges of the gain medium. Recently, a new method for growing large scale Yb:YAG crystals with clear aperture larger than 140 mm was introduced by a crystal growing company Crytur [9] and, together with optical bonding of Cr:YAG absorber onto the crystal, such crystals slabs can be used for high energy high repetition rate laser systems. Monocrystals allow depolarization control due to uniform crystal orientation [10]. Due to polycrystalline nature of ceramics, such control is not possible and therefore the high power laser community still puts a lot of effort into monocrystals development. In this article, we use the first cryogenic main pre-amplifier of the Bivoj/DiPOLE capable of delivering pulses with energy up to 10 Joules to directly compare multiple Yb:YAG sets of gain media from ceramics or monocrystals to our knowledge for the first time at these high energy levels and repetition rates. Output energy for Yb:YAG crystal without ASE absorber and ceramics with ASE absorber was compared at 14 J and 2 Hz at LUCIA [11] and small signal gain comparison for Nd:YAG crystal and Nd:LuAG ceramics was performed at 10 Hz [12]. In addition to absorption-based ASE countermeasures, we also tested a prototype one based on surface structuring of the gain media and compared them all with plain slabs with no ASE suppression.

2. System layout

The DiPOLE/Bivoj system [13] incorporates a low-energy, fiber-based front end oscillator (~ nJ), followed by a regenerative Yb:CaF_2 amplifier that increases the output energy to the mJ level (PA1) and a rod Yb:YAG multi-pass booster amplifier to raise the output energy to multi tens mJ level (PA2). Two diode pumped, helium gas cooled large aperture power amplifiers then increase the output energy to 7 J (Main pre-Amplifier 1) and finally to 100 J (Main power Amplifier 2). The schematic of the system is in Fig. 1.

The front end starts with a single frequency temperature stabilized tunable CW fiber oscillator. The CW beam is then temporarily shaped in an A-O (acousto-optic) modulator to produce 200 ns long pulses with a repetition rate of 10 kHz. Pulses are then amplified in a fiber amplifier and subsequently shaped by an E-O (electro-optic) modulator to produce 2-14 ns pulses with arbitrary shape and a resolution of 200 ps. The output energy is around 10 nJ for a 10 ns long pulse. Then the pulses are sent to regenerative rod amplifier (PA1, Amplitude Systemes) based on Yb:CaF_2 that reduces repetition rate to 10 Hz and boosts the energy to ~4 mJ. The 2 mm Gaussian beam coming from the regenerative amplifier is then spatially shaped to a 8 mm × 8 mm square super-Gaussian profile in a beam shaper consisting of π-shaper and serrated aperture with a spatial filter. Then the pulse is further amplified to ~50 mJ in a 6-pass booster amplifier (PA2, Lastronics GmBH) based on Yb:YAG. The booster amplifier preserves the square super-Gaussian beam profile, which is subsequently expanded to 21 mm × 21 mm and injected into the 10 J main pre-amplifier.

The 10 J main pre-amplifier (MA1) is based on a multi-slab design. It consists of four circular Yb:YAG slabs with two doping levels of Yb (1.1 at.% for outer slabs, 2.0 at.% for inner slabs). The dimensions of each circular slab are 45 mm in diameter and 5 mm in thickness. The Yb:YAG is cladded with a 5 mm Cr:YAG absorber (absorption coefficient of 6 cm^{-1}) which minimizes loses due to ASE and parasitic oscillations. The pumped area is a square of 23 mm × 23 mm. The pump beam is coming from two homogenized, diode pump modules operating at 939 nm and each producing 29 kW of peak power in up to 1200 µs long laser pulses at a repetition rate of 10 Hz. The amplifier is cooled by a forced Helium gas flow with a pressure around 8 bar at a

Optics EXPRESS

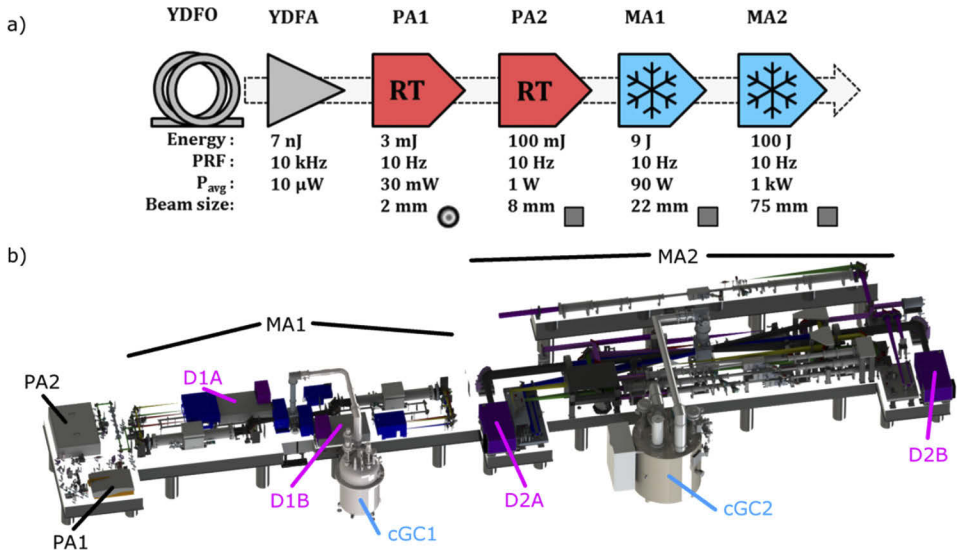

Fig. 1. (a) Schematic of Bivoj/DiPOLE100 amplifier chain showing maximum output performance after each amplifier stage, including free-space beam size and shape: YDFO = Yb-silica fiber oscillator; YDFA = Yb-silica fiber amplifier (inc. temporal pulse shaping); PA = room-temperature pre-amplifier (1 = Yb:CaF_2 regenerative, 2 = Yb:YAG multi-pass); MA = main cryogenic amplifier (ceramic Yb:YAG multi-slab). (b) 3D model of DiPOLE100 system: D = Diode pumps; cGC = cryogenic gas coolers (Ref. [6], Fig. 1).

temperature of 150 K. The head housing the gain media is separated from the vacuum isolation by sapphire pressure windows and the isolation vacuum from the ambient environment by fused silica vacuum windows.

The beam is injected into the amplifier through a dichroic mirror and then is image-relayed by a spatial filter (f = 0.9 m) to a back reflector and then relay-imaged back to the amplifier head. Each pass is propagated by a set of separate mirrors and lenses. A square bimorph deformable mirror with 49 actuators and dielectric coating (Adaptica 7 × 7, 27 mm × 27 mm, stroke ± 30 µm) is placed in the amplifier after the 3rd pass. This mirror, together with lens arrays placed on linear stages, is used to compensate the thermal wavefront distortion acquired in the amplifier head. The birefringence of the sapphire pressure windows changes the polarization of the beam and sets of quarter- and half-waveplates are used to compensate this on pass 1 and 5. The beam exits the amplifier after 7 passes.

3. Gain media comparison

To compare all gain media, we first inspected them in the laboratory to evaluate the level of scattering before insertion into the amplifier head. Then we measured the small signal gain (SSG) and amplification to maximum achievable energy. We also measured thermal aberrations caused by the slabs in the form of wavefront distortion. For ceramics and cladded crystals, we also calculated the wavefront distortion numerically.

3.1. Gain media

The parameters of the gain media slabs are summarized in Table 1. All slabs had an outer diameter of 55 mm. The Yb:YAG aperture was 45 mm for the ceramics, 37 mm for the cladded monocrystals, full aperture of 55 mm for the un-cladded plain monocrystals, and 37 mm for the structured monocrystals. The smaller clear aperture of the cladded monocrystals was caused by a

Optics EXPRESS

hexagonal shape of Yb:YAG part, which was necessary for optical bonding of Cr:YAG absorber cladding.

Table 1. Overview of gain media parameters

Parameter	Ceramics	Monocrystals		
		Cladded	Plain	Structured
Yb doping (at. %)	1.1% and 2%	1.1% and 2%	1.1% and 2%	1.1% and 2%
Orientation	random	[100]	[100]	[100]
Cr absorption[cm^{-1}]	6, 6.35, 6.35, 6.45	6.1	NA	NA
Total thickness [mm]	19.88	21.09	21.89	21.83
Clear aperture [mm]	35	37	55	37

To visually assess the quality of the gain media, we observed them in collimated bright light. Photographs from this observation taken with same exposition settings of a camera are shown in Fig. 3. All slabs show scattering of the light in the clear aperture, but the visual levels are small and comparable.

The micro-structure was a series of equidistantly spaced concentric rings (see Fig. 2), where material was removed by laser ablation. A comparable structure is used by Crytur to enhance out-coupling of a light generated in Cr:YAG scintillators. In our home-made code using Monte Carlo approach, we calculated that the structure increases out-coupling efficiency for very broad spectral range. In the scintillators, the light radiated from the crystal increases by 300-400% when one of the faces is micro-structured. Additionally, mean free path of the rays in the scintillator decreases 10 times, when one surface is micro-structured. These properties of the scintillators were the primary motivation for trying similar micro-structuring as ASE prevention in laser slabs.

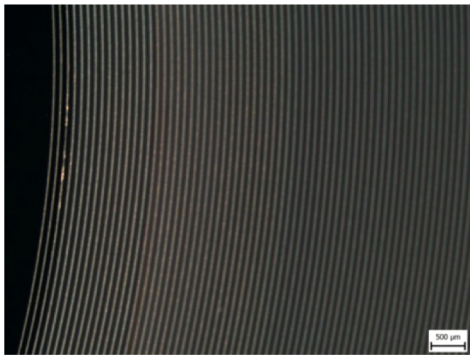

Fig. 2. Photographs of the micro-structure with 20 times magnification from optical microscope.

3.2. Small signal gain measurement

In this experiment, the gain media were pumped by a total energy of 50 J in a 1 ms long pulse centered at 939.5 nm at a 1 Hz and 10 Hz repetition rate. The 10 ns signal pulse attenuated to 5 mJ coming from PA2 was amplified in a single pass through the amplifier head. The input and output pulse energy was simultaneously monitored by energy meters (input: Gentec QE25LP in leakage through a high reflectivity mirror, output: QE50LP directly in the beam). The gain was measured at two temperatures, 120 K and 150 K. In each measurement, the signal wavelength was adjusted to the peak of the gain curve for each temperature.

Optics EXPRESS

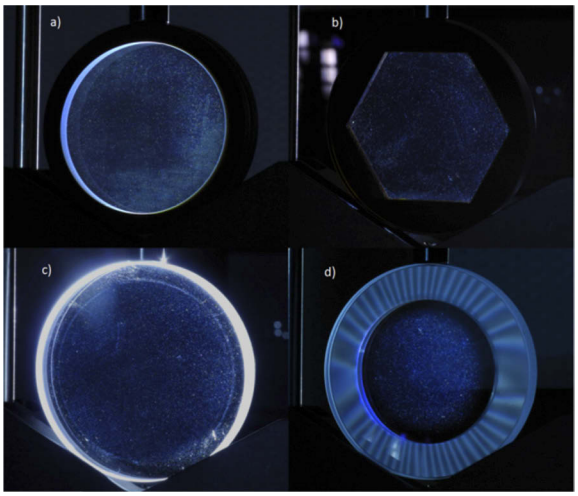

Fig. 3. Photographs of the gain media taken with 0.5 s exposure for a) ceramics, b) cladded monocrystals, c) plain monocrystals, and d) structured monocrystals.

During the measurement, the delay between the pump and signal pulses was changed, so the signal pulse observed a different effective pump energy, but the heat load of the amplifier remained constant. The ratio of input and output energies give the small signal gain values, which are summarized in Fig. 4.

The SSG is heavily influenced by ASE, therefore slabs with ASE absorbers show better results than plain slabs. Structured slabs performed poorly in this comparison, effectively on the same level as the plain monocrystals. We noticed that ASE coming out of the amplifier was roughly three times higher for structured slabs in comparison to other gain media sets, which would be in line with initial predictions. However the reason for their poor performance is still not clear. The temperature of the slabs also influences the SSG, with lower temperatures producing a higher emission cross-section and thus higher gain if ASE is suppressed, as in the case of the ceramics and cladded monocrystals. Conversely, if ASE is not suppressed, lower temperature decrease the gain even below the value obtained at higher temperatures, as in the case of the structured and plain monocrystals. The small discrepancy between ceramics and cladded monocrystals at 10 Hz pumping probably originates from the higher inner temperature of cladded monocrystals as will be explained later. The highest values of SSG are summarized in Table 2.

Table 2. Maximum SSG values for different temperatures and repetition rates.

Temperature	120 K		150 K	
Rep. rate	1 Hz	10 Hz	1 Hz	10 Hz
Ceramics	6.05	4.75	4.3	3.6
Cladded monocrystals	5.8	4.5	4.2	3.5
Structured monocrystals	2.1	2.45	2.4	2.5
Plain monocrystals	1.8	1.85	2.05	2.1

3.3. Amplification and wavefront aberrations

After the SSG measurement, the beam was propagated through the whole amplifier and the output energy was measured. The amplifier was realigned completely with each new slab set. The energy output from PA2 was increased to 30 mJ and the pulse duration remained 10 ns. In this

Optics EXPRESS

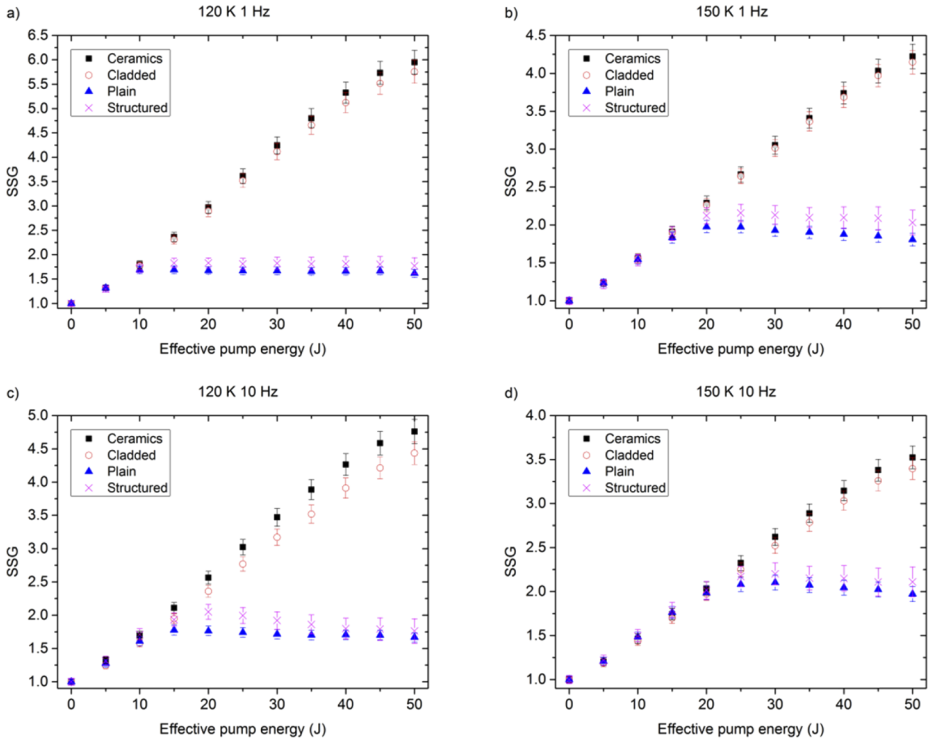

Fig. 4. Small signal gain for various temperatures and repetition rates a) 1 Hz 120 K, b) 1 Hz 150 K, c) 10 Hz 120 K, and d) 10 Hz 150 K for ceramics (square), cladded monocrystals (circle), plain monocrystals (triangle), and structured monocrystals (cross).

experiment, the gain media were pumped by a total energy of 30 J in a 600 µs long pulse (same peak power as in SSG measurement) centered at 939.5 nm at 1 Hz and 10 Hz repetition rates. We chose shorter pump pulse duration than what is used in regular operation to decrease the thermal loading of the amplifier and still be able to reach 6 J of output energy. The temperature of the amplifier was set to 150 K. Lower temperatures weren't used, since self-lasing was observed at lower temperatures. Results are summarized in Fig. 5.

Before amplification, we set the lens arrays to positions where thermal lensing is not compensated, and the deformable mirror to a flat surface. We captured wavefronts at the output of the amplifier with no pumping, and then captured the wavefronts again while pumping. Then we changed the delay between signal and pump pulse to obtain amplification and captured wavefronts. By subtracting the corresponding wavefronts, we characterized the thermal lens at full thermal load with no energy extraction and at maximum energy extraction. Then the lens arrays and deformable mirror surface were optimized to obtain the lowest aberrations on the beam, captured wavefronts, and near and far field profiles.

Wavefronts reflecting thermal lenses (Fig. 6) and beam profiles for optimized wavefront (Fig. 7) and are presented only for 10 Hz operation, because at 1 Hz all profiles are less affected by heat and show even less difference. The optimized wavefronts for all slab sets have similar peak to valley (P-V) values below 0.8 µm and RMS below 0.08 µm, therefore they are not presented here. All images were taken from a leak through a high reflective mirror. The leaked beam was down-collimated (1:10) and then imaged onto a detector (near fields, wavefronts) or focused by f = 100 mm lens (far fields).

Optics EXPRESS

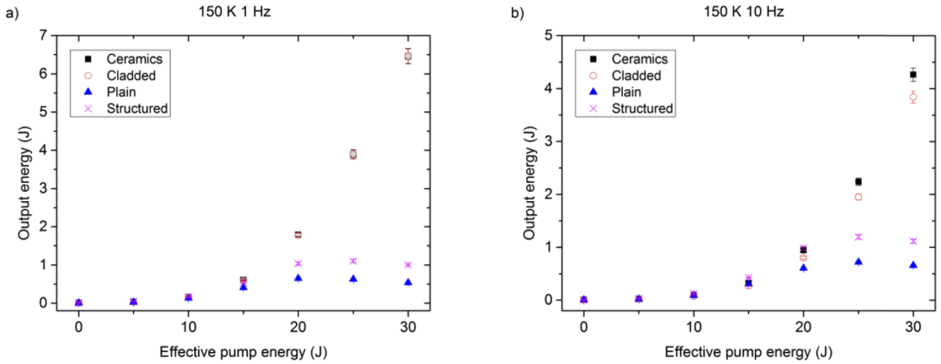

Fig. 5. Amplification of 10 ns, 30 mJ signal beam in amplifier with ceramics (square), cladded monocrystals (circle), plain monocrystals (triangle), and structured monocrystals (cross) at temperature of 150 K for pumping at a) 1 Hz repetition rate and b) 10 Hz repetition rate.

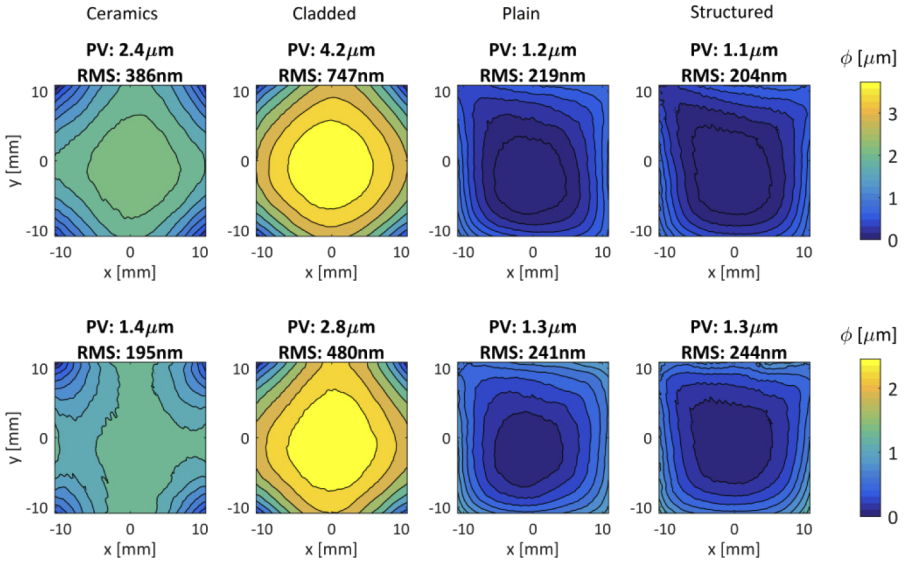

Fig. 6. Wavefronts at the output of the system for (top row) full thermal load with no energy extraction and for (bottom row) thermal load lowered by maximum energy extraction from the amplifier. Wavefronts correspond from left to right to ceramics, cladded monocrystals, structured monocrystals, and plain monocrystals.

The maximum output energy correlates with the SSG measurements. For 1 Hz operation, the differences are smaller, the ceramics reached 6.5 J, the cladded monocrystals reached also 6.5 J, while the structured monocrystals reached only 1.05 J and the plain monocrystals only 0.65 J. For 10 Hz operation, the differences are larger and follow the previous trends, the ceramics reached 4.3 J, the cladded monocrystals reached 3.9 J, while the structured monocrystals reached only 1.2 J and the plain monocrystals only 0.7 J. The cladded monocrystals show lower output energy probably due to the higher temperature of the active area, which was calculated to be 1.5-2.5 degrees above the ceramics due to closer proximity of the absorber to the beam. The structured monocrystals had a higher output energy at 10 Hz operation due to increased

Optics EXPRESS

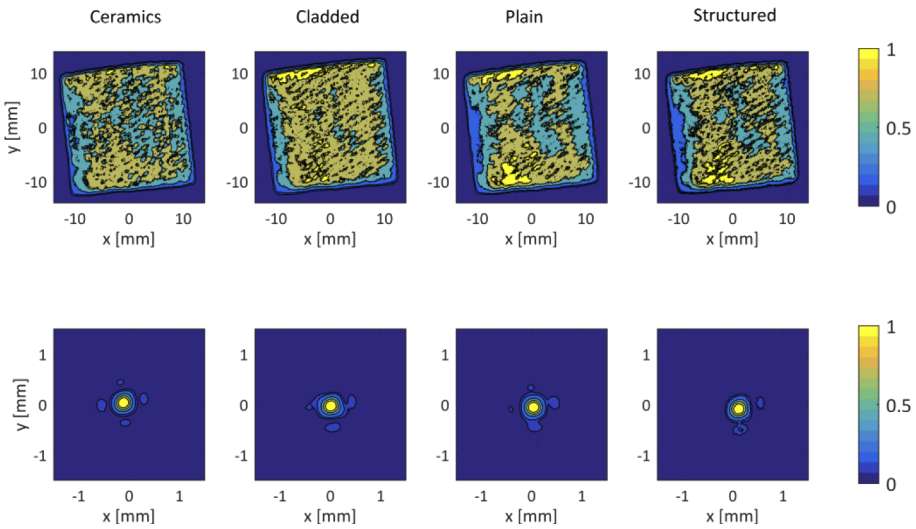

Fig. 7. Near field (top) and far field (bottom) beam profiles for maximum output energy with optimized wavefront at 10 Hz operation for from left to right ceramics, cladded monocrystals, structured monocrystals, and plain monocrystals.

temperature that lowered ASE due to higher re-absorption and lower emission cross-section. Similar behavior is observed for plain slabs.

Note that the output energies of the structured monocrystals are 71% and 61% higher than the output energies of the plain monocrystals at 10 Hz and 1 Hz, respectively. Both values of the structured monocrystals are well below the values of the cladded monocrystals and the ceramics. This point deserves some further attention, which would, however, go beyond the scope of this paper.

The thermal lens reflects the amount of heat generated in the slab. Slabs without an absorber layer have the opposite sign for the thermal lens in comparison to slabs with an absorber. Since most of the heat is generated in the absorber itself, it changes the thermal lens sign easily. The cladded monocrystalline slabs show largest thermal lens of all sets, which is a result of the close proximity of the absorber and the pumped area of the Yb:YAG.

3.4. Thermal calculations

The experimentally obtained thermal lenses and assumptions about temperature of the slabs were compared with a numerical model. We used a MATLAB code [14,15] to calculate the heat generated in the slabs. We note that the MATLAB code is not able to calculate heat in the slabs without an absorber, since it relies on Monte Carlo ray tracing and absence of the cladding will trap rays in the slab and cause very long computation times. Simple assumptions would yield faulty results, so we do not present data for slabs without an absorber here. The calculated heat distribution was then imported to COMSOL to model temperature profiles and the thermal lenses in the slabs in the amplifier head. In accordance with experiment, the coolant temperature was set to 150 K, He pressure to 7.5 bar with flow of 30 m^3/h. The ceramic slabs were thinner (5 mm) than the cladded monocrystals (5.27 mm) which mean the separation between ceramic slabs was larger than between the cladded monocrystalline slabs. This increased gap between ceramics slabs resulted in a decreased flow velocity of He between the slabs and a lower calculated heat transfer coefficient for the cladded ceramic slabs (1500 W/m^2/K) in comparison to the cladded monocrystalline slabs (1800 W/m^2/K). For calculations we assumed that He flow was turbulent and there was no contact of the slab with the holder. For 300 W pumping, in case of full thermal

Optics EXPRESS

lens, the calculated heating in the pumped volume of the slabs was 28.5 W and in the absorber cladding 246 W. For full energy extraction it was 28.5 W and 186 W, respectively. The absorption coefficient of the absorber was chosen to be 6 cm^{-1} in both cases. The surface temperature profiles of the slabs are shown in Fig. 8.

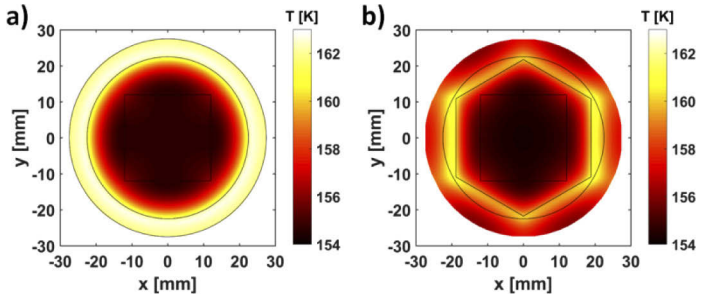

Fig. 8. Temperatures on the surface of the slab at 10 Hz pumping with maximum energy extraction for a) ceramics and b) cladded monocrystals. Black square in the picture represents pumped area of the slab.

Thermal calculations also predict that the average temperature in the pumped area rises to 154 K for ceramics and to 155.5 K for cladded monocrystals. The maximum temperature rises to 155.5 K for ceramics and to 157.5 K for cladded monocrystals. Both calculated for maximum energy extraction from the amplifier. The temperatures are even higher in the case of no energy extraction (average temperatures 158.5 K and 160 K, maximum temperatures 160.5 K and 163.5 K for ceramics and cladded crystal, respectively).

The calculated wavefront of the beam after 7 passes through the amplifier head pumped at 10 Hz with no energy extraction is shown in Fig. 9. Peak to valley values of the wavefront with no energy extraction and for maximum energy extraction are summarized in Table 3. All show good match to experimentally obtained values and in shape and confirm our model of the gain medium.

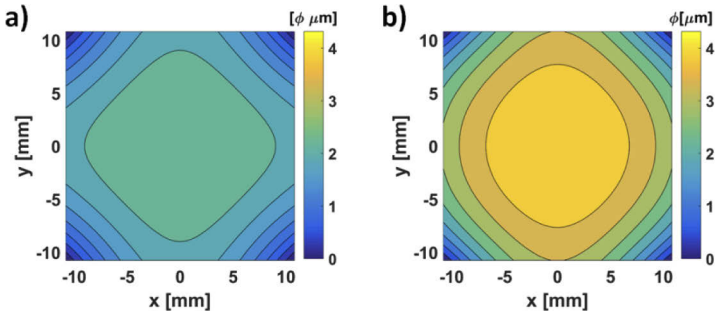

Fig. 9. Calculated wavefront after 7 passes through amplifier head pumped at 10 Hz with no energy extraction for a) ceramics and b) cladded monocrystals.

Table 3. Calculated P-V values of wavefronts measured with 10 Hz pumping

Slab	Wavefront P-V value full thermal lens		Wavefront P-V value max energy extraction	
	Measured [μm]	Calculated [μm]	Measured [μm]	Calculated [μm]
Ceramics	2.4	2.48	1.4	1.35
Cladded crystal	4.2	4.32	2.8	2.73

Optics EXPRESS

4. Summary

We compared several types of slab gain media based on Yb:YAG in a 10 J, 10 Hz laser system (cladded ceramics, and cladded, structured and plain monocrystals). ASE suppression had a large influence on the performance of the amplifier, and Cr:YAG absorbers were much better than micro-structured treatment of the surface of the slabs. Minor performance effects were observed due to the different geometry of the monocrystalline and ceramics claddings. For similar geometries, the performance is expected to be the same.

We therefore conclude that the performance of cladded single crystal in a large area high average power amplifier is the same as of ceramics. This should grant the laser community more flexibility in laser design and in sourcing gain media for high energy amplifiers.

Funding

European Regional Development Fund (CZ.02.1.01/0.0/0.0/15_006/0000674, CZ.02.1.01/0.0/0.0/16_019/0000789); H2020 Spreading Excellence and Widening Participation (739573); Ministerstvo Školství, Mládeže a Tělovýchovy (LO1602).

Disclosures

Jana Preclikova, Jan Kubat: Crytur s.r.o. (E) and Jindrich Houzvicka: Crytur s.r.o. (I, E). The authors declare that there are no conflicts of interest related to this article.

References

1. P. J. Mallozzi and B. P. Fairand, "Altering Material Properties," U.S. Patent 3,850,698, (1974).
2. A. Azhari, S. Sulaiman, and A. K. Prasada Rao, "A review on the application of peening processes for surface treatment," IOP Conf. Ser.: Mater. Sci. Eng. **114**, 012002 (2016).
3. C. M. Brenner, S. R. Mirfayzi, D. R. Rusby, C. Armstrong, A. Alejo, L. A. Wilson, R. Clarke, H. Ahmed, N. M. H. Butler, D. Haddock, A. Higginson, A. McClymont, C. Murphy, M. Notley, P. Oliver, R. Allott, C. Hernandez-Gomez, S. Kar, P. McKenna, and D. Neely, "Laser-driven x-ray and neutron source development for industrial applications of plasma accelerators," Plasma Phys. Controlled Fusion **58**(1), 014039 (2016).
4. A. Bayramian, J. Armstrong, G. Beer, R. Campbell, B. Chai, R. Cross, A. Erlandson, Y. Fei, B. Freitas, R. Kent, J. Menapace, W. Molander, K. Schaffers, C. Siders, S. Sutton, J. Tassano, S. Telford, C. Ebbers, J. Caird, and C. Barty, "High-average-power femto-petawatt laser pumped by the mercury laser facility," J. Opt. Soc. Am. B **25**(7), B57–B61 (2008).
5. C. L. Haefner, A. Bayramian, S. Betts, R. Bopp, S. Buck, J. Cupal, M. Drouin, A. Erlandson, J. Horacek, J. Horner, J. Jarboe, K. Kasl, D. Kim, E. Koh, L. Koubikova, W. Maranville, C. Marshall, D. Mason, J. Menapace, P. Miller, P. Mazurek, A. Naylon, J. Novak, D. Peceli, P. Rosso, K. Schaffers, E. Sistrunk, D. Smith, T. Spinka, J. Stanley, R. Steele, C. Stolz, T. Suratwala, S. Telford, J. Thoma, D. VanBlarcom, J. Weiss, and P. Wegner, "High average power, diode pumped petawatt laser systems: a new generation of lasers enabling precision science and commercial applications," Proc. SPIE **10241**, 1024102 (2017).
6. P. Mason, M. Divoký, K. Ertel, J. Pilař, T. Butcher, M. Hanuš, S. Banerjee, J. Phillips, J. Smith, M. D. Vido, A. Lucianetti, C. Hernandez-Gomez, C. Edwards, T. Mocek, and J. Collier, "Kilowatt average power 100 J-level diode pumped solid state laser," Optica **4**(4), 438–439 (2017).
7. R. Yasuhara, T. Kawashima, T. Sekine, T. Kurita, T. Ikegawa, O. Matsumoto, M. Miyamoto, H. Kan, H. Yoshida, J. Kawanaka, M. Nakatsuka, N. Miyanaga, Y. Izawa, and T. Kanabe, "213 W average power of 2.4GW pulsed thermally controlled Nd:glass zigzag slab laser with a stimulated Brillouin scattering mirror," Opt. Lett. **33**(15), 1711–1713 (2008).
8. T. Liu, Z. Sui, L. Chen, Z. Li, Q. Liu, M. Gong, and X. Fu, "12 J, 10 Hz diode-pumped Nd:YAG distributed active mirror amplifier chain with ASE suppression," Opt. Express **25**(18), 21981–21992 (2017).
9. J. Preclíková, K. Bartoš, J. Kubát, M. Košelja, B. Rus, M. Divoký, T. Mocek, and J. Houžvička, "Large Scale Single Crystal Growth," in *Laser Congress 2018 (ASSL)*, OSA Technical Digest (Optical Society of America, 2018), paper AM4A.1.
10. M. Azrakantsyan, D. Albach, N. Ananyan, V. Gevorgyan, and J.-C. Chanteloup, "Yb^{3+}:YAG crystal growth with controlled doping distribution," Opt. Mater. Express **2**(1), 20–30 (2012).
11. T. Gonçalvès-Novo, D. Albach, B. Vincent, M. Arzakantsyan, and J.-C. Chanteloup, "14 J / 2 Hz Yb3+:YAG diode pumped solid state laser chain," Opt. Express **21**(1), 855–866 (2013).
12. T. Liu, T. Feng, Z. Sui, Q. Liu, M. Gong, L. Zhang, B. Jiang, and X. Fu, "50 mm-aperture Nd:LuAG ceramic nanosecond laser amplifier producing 10 J at 10 Hz," Opt. Express **27**(11), 15595–15603 (2019).

Optics EXPRESS

13. S. Banerjee, P. D. Mason, K. Ertel, P. J. Phillips, M. De Vido, O. Chekhlov, M. Divoky, J. Pilar, J. Smith, T. Butcher, A. Lintern, S. Tomlinson, W. Shaikh, C. Hooker, A. Lucianetti, C. Hernandez-Gomez, T. Mocek, C. Edwards, and J. L. Collier, "100 J-level nanosecond pulsed diode pumped solid state laser," Opt. Lett. **41**(9), 2089–2092 (2016).
14. M. Sawicka, M. Divoky, J. Novak, A. Lucianetti, B. Rus, and T. Mocek, "Modeling of amplified spontaneous emission, heat deposition, and energy extraction in cryogenically cooled multislab Yb3+:YAG laser amplifier for the HiLASE Project," J. Opt. Soc. Am. B **29**(6), 1270–1276 (2012).
15. M. Sawicka, M. Divoky, A. Lucianetti, and T. Mocek, "Effect of amplified spontaneous emission and parasitic oscillations on the performance of cryogenically-cooled slab amplifiers," Laser Part. Beams **31**(4), 553–560 (2013).